PRC1 and EB1 Binding Dynamics Reveal a Solidifying Central Spindle during Anaphase Compaction in Human Cells

Jayant Asthana[1,2], Nicholas I. Cade[1,&], Wei Ming Lim[1,2], Thomas Surrey[1,2,3,#]

[1] The Francis Crick Institute, 1 Midland Road, London, NW1 1AT, UK
[2] Centre for Genomic Regulation (CRG), Barcelona Institute of Science and Technology (BIST), Dr Aiguader 88, 08003 Barcelona, Spain
[3] ICREA, Passeig de Lluis Companys 23, 08010 Barcelona, Spain

[&] Present address: UK Dementia Research Institute at UCL, Gower Street, London WC1E 6BT, UK

[#] Correspondence:
thomas.surrey@crg.eu

ABSTRACT

During mitosis the spindle undergoes considerable morphological and dynamic changes. Particularly the central spindle reorganizes drastically at the onset of anaphase when the antiparallel microtubule bundler PRC1 starts to accumulate and recruit a subset of spindle proteins to the midzone. Little is known about how the dynamic properties of the central spindle change during its morphological changes in human cells. Using CRISPR/Cas9 gene editing, we generated human RPE1 cells that express from their endogenous locus fluorescently tagged versions of the two cytoskeletal network hub proteins PRC1 and the end binding protein EB1 to be able to quantify their spindle distribution and binding/unbinding turnover under native conditions. We find that throughout mitosis EB1 binds central spindle microtubule bundles in a PRC1-dependent manner using a binding mode different from EB1 at growing microtubule ends. Both proteins, PRC1 and EB1, progressively accumulate and bind increasingly strongly to compacting central antiparallel microtubule overlaps. These results show that the central spindle gradually 'solidifies' during mitosis, suggesting that the two protein interaction networks around PRC1 and EB1 cooperate to stabilize the shortening central spindle, explaining the importance of both proteins for correct chromosome segregation and cytokinesis.

KEYWORDS

Mitosis, PRC1, EB1, midzone, spindle dynamics, gene-editing, CRISPR/Cas9, RPE1, FRAP

INTRODUCTION

During cell division, the mitotic spindle that is responsible for segregating the two sets of chromosomes to the new daughter cells, undergoes dramatic morphological changes. During anaphase which lasts ~ 10 min in animal cells, chromosomes are pulled to the spindle poles, while the spindle dynamically reorganises and elongates[1]. At the same time, microtubules that constitute major elements of the spindle become more stable, with their average lifetimes decreasing from ~ 20 s in metaphase to several minutes in anaphase and telophase[2-6]. Concomitantly, the spindle concentrates antiparallel microtubule overlaps in its centre, a region also called the midzone, that is critically important for spindle stability and function, as well as for intracellular signalling events ensuring correct cytokinesis[7, 8]. The molecular mechanisms underlying the changes of spindle morphology and internal spindle dynamics are, however, only poorly understood.

The mirror-symmetric structure of the spindle is enforced by antiparallel microtubule overlaps stabilised by microtubule-crosslinking proteins. PRC1 (Protein Regulator of Cytokinesis 1) is an evolutionary conserved crosslinker that specifically connects microtubules in an antiparallel configuration[9-11]. In metaphase, PRC1 localises to "bridging fibres" which are mixed polarity microtubule bundles connecting opposing sister kinetochore fibres[12, 13]. As the spindle reorganises in anaphase as a consequence of the decreasing activity of Cdk1/cyclin B kinase, PRC1 is dephosphorylated and concentrates at the forming spindle midzone[14-22]. PRC1 also recruits several other midzone proteins, including kinesins, kinases and signalling proteins[23-25]. Together they stabilize the central antiparallel microtubule overlaps which have a length of ~ 2 µm in animal cells[16, 17, 26, 27]. However, little quantitative information exists about how PRC1 redistributes in the spindle over the entire duration of mitosis, particularly under conditions of non-overexpressed protein. Whereas the dynamic properties of the conserved PRC1 homolog Ase1 have been investigated in budding yeast spindles[28], much less is known about its binding/unbinding turnover on microtubules during different stages of mitosis in animal cells[17], limiting our understanding of the structure and dynamic properties of the spindle during its reorganization in mitosis.

Another important cellular recruitment factor for the microtubule cytoskeleton is the end binding protein EB1[23, 29]. EB1 family members (EBs) track growing microtubule plus ends dynamically, with their N-terminal calponin homology domain binding preferentially to the growing part of microtubules where the GTP cap is[30-36]. Their C-terminal EB homology (EBH) domain recruits binding partners that either contain a CAP-Gly domain or a linear sequence motifs such as a SxIP motif [37, 38]. Interestingly, some EB1 interactors are also known interaction partners of PRC1[39-42]. EB1 end tracking is a very dynamic process with characteristic single molecule dwell times being in the range of hundreds of milliseconds[32, 34, 43]. EB1 proteins are often used as ectopically expressed fluorescent microtubule end markers in living cells[33, 44-46]. The localization pattern of EB1 in mitotic spindles is however not clear. Depending on the studied cell type and the method of visualization, EBs were reported to either exclusively track growing microtubule ends[17, 45, 47-51] or to localize also to central

microtubule bundles in both metaphase and anaphase[28, 52-56]. This localization to the central anaphase spindle could be a reflection of reports of end binding proteins playing a role in promoting correct cytokinesis[42, 57, 58].

Here, we examined the distribution and the dynamic properties of PRC1 and EB1 in spindles of diploid human cells during mitosis. To allow measurements under close-to-native conditions, we engineered RPE1 cells using CRISPR/Cas9 gene-editing technology to express fluorescently tagged PRC1 and EB1 from their endogenous genetic loci. We quantified the redistribution of PRC1, imaging the transformation of bridging fibres in metaphase to central midzone bundles in anaphase and telophase. We found that PRC1 turnover slowed down dramatically, as microtubule overlaps compacted. We also found that EB1 bound to the central spindle in a PRC1-dependent manner, provided that it can interact with its binding partners. This binding mode differs from its microtubule end tracking mode as EB1 displays also strongly reduced binding/unbinding turnover in the compacting central spindle. These results suggest, that the protein interaction networks of both hub proteins PRC1 and EB1 are interlinked in mitosis and both contribute to solidify the central spindle as mitosis proceeds.

RESULTS

Antiparallel microtubule overlaps marked by PRC1 shorten during mitosis as the spindle elongates

To be able to monitor central spindle characteristics during mitosis using fluorescently labelled PRC1 expressed at natural levels, we gene-edited hTERT-RPE1 cells using CRISPR/Cas9 technology to insert a monomeric GFP (mGFP) gene at the 5' end of the PRC1 gene. Genotypic analysis of single cell clones showed that the mGFP gene was inserted at the correct genomic locus (Suppl. Fig. 1A) and that both PRC1 alleles were modified (Suppl. Fig. 1B). Consequently, all expressed PRC1 molecules, including different splice isoforms, carry a N-terminal mGFP tag in these cells. The clone that expressed the most similar level of fluorescently tagged PRC1 compared to untagged PRC1 in control cells (Suppl. Fig. 1C) was selected for further studies (Suppl. Table 1).

We first imaged mGFP-PRC1 expressed from its endogenous locus in gene-edited cells over the time course of mitosis in the presence of the DNA marker Hoechst. To synchronise the cells, they were arrested before mitosis at the G1/S transition by the addition of thymidine and then released by thymidine removal. As soon as the nuclear envelope broke down, indicative of the beginning of prophase, PRC1 started to localize to the spindle (Fig. 1A, Suppl. Movie 1). During metaphase when chromosomes were aligned in the spindle centre, PRC1 localized evenly to microtubule bundles throughout the entire spindle, as noted previously by immunostaining PRC1 in fixed cells[15, 19, 59] or by visualising over-expressed GFP-tagged PRC1 in bridging fibres of metaphase spindles in live cells [12, 13]. Over the time course of anaphase when chromosomes were segregating, PRC1 became more confined to

the central spindle where it selectively accumulated (Fig. 1A, Suppl. Movie 1), as observed previously using either immunostaining or overexpressing fluorescently labelled PRC1[14-19, 22, 27]. In telophase, PRC1 strongly accumulated at the midbody (Fig. 1A, Suppl. Movie 1), as expected[20, 22].

Individual kymographs (space-time plots) generated along the pole-to-pole axis of the spindle and an average kymograph generated from 17 individual spindles illustrate the strong accumulation of PRC1 in the spindle centre during anaphase (Fig. 1B, Suppl. Fig. 2A). mGFP-PRC1 and DNA intensity profiles obtained from the average kymographs show that after chromosomes started to separate, the PRC1 profile transformed from a roughly Gaussian distribution in metaphase to a distribution with one central peak and two lower shoulders or side peaks (Fig. 1C, Suppl. Fig. 2B). The central PRC1 peak represents the midzone with antiparallel microtubules, whereas the side peaks likely represent spindle regions with mostly parallel microtubules to which PRC1 binds only weakly. Fitting these anaphase profiles using a sum of three Gaussians allowed us to extract the time evolution of both the overall spindle length and the central antiparallel overlap length (Fig. 1D, Methods).

During the first ~ 5 min of anaphase, spindles in these RPE1 cells extended from an initial length of ~ 8 μm roughly at the same rate as chromosomes separated up to a maximum length of 20 μm (Fig. 1D). After the start of cytokinetic furrow ingression (at ~ 4 min of anaphase, not shown) the chromosomes continued to separate more slowly while spindle length did not change anymore. The central antiparallel microtubule overlaps shortened initially fast (although their exact length could not be reliably extracted from our fits until ~ 3 min of anaphase) and then slowly approached a final length of ~ 1.7 μm (full width at half maximum FWHM) (Fig. 1D), in agreement with previous measurements in Hela and RPE1 cells using overexpressed fluorescently tagged PRC1[17]. The density of the PRC1 molecules in the midzone increased strongly after about 3 min of anaphase as indicated by a strong increase of the central peak intensity of the PRC1 profile (Fig. 1D), as observed previously for overexpressed PRC1[16, 27]. These results indicate that the PRC1 binding strength to the central midzone increases over time of anaphase. Taken together, our data demonstrate that in cells with natural PRC1 expression levels, the length of antiparallel microtubule overlaps continuously decreases towards a final end length in the micrometer range as PRC1 becomes more and more concentrated in the spindle midzone.

PRC1 turnover decreases as the central spindle compacts

Recently the binding/unbinding turnover of ectopically expressed GFP-PRC1 in an anaphase RPE1 cell was found to be slow, with a fluorescence recovery time after photobleaching (FRAP) of several tens of seconds[17]. To determine how the dynamics of PRC1 binding to the central spindle develops during mitosis, we performed FRAP experiments using gene-edited RPE1 cells expressing mGFP-PRC1 from its endogenous locus at different mitotic stages (Fig. 2A). Average intensity profiles of mGFP-PRC1 and Hoechst-stained DNA, visualizing the extent of midzone compaction and chromosome position, respectively (Fig. 2B), together with the corresponding average mGFP-PRC1 fluorescence recovery curves at the different

stages of mitosis were generated from at least 15 individual bleached spindles per condition (Fig. 2C). We observed that the recovery time decreased continuously during the course of mitosis, with values of 6.1 ± 0.2 s, 11 ± 0.6 s, 11 ± 0.4 s, 44 ± 3 s and 124 ± 20 s measured in metaphase, early anaphase, mid-anaphase, late anaphase and telophase, respectively (Fig. 2D, E, Suppl. Movie 2). A similar trend was observed previously for the PRC1 orthologue Ase1 in budding yeast spindles [28]. These results demonstrate that the binding/unbinding turnover of PRC1 slows down the more PRC1 concentrates and accumulates at the central spindle region, indicative of a gradual solidification of the central part of the spindle as mitosis proceeds until hardly any PRC1 turnover is measurable at the midbody in telophase.

Endogenous mGFP-EB1 colocalizes with PRC1 to the central spindle

To investigate the morphology of the central spindle and simultaneously the growth dynamics of microtubules during mitosis, we generated hTERT-RPE1 cell lines in which both PRC1 and EB1 were fluorescently tagged at their endogenous locus using CRISPR/Cas9 gene editing. We first generated a cell line with a mGFP gene inserted at the 5'-end of the EB1 gene, and then additionally inserted a mCherry gene at the 5'-end of the PRC1 gene. Genotypic analysis of single cell clones showed that mGFP and mCherry genes were inserted at the correct genomic locus (Suppl. Fig. 3A, 3D) and that both EB1 and PRC1 alleles were modified (Suppl. Fig. 3B, 3E). Western blot analysis showed that mGFP-EB1 was about twofold less abundant than untagged EB1 in control RPE1 cells (Suppl. Fig. 3C). As observed for our mGFP-PRC1 cells, mCherry-PRC1 expressed at similar levels compared to untagged PRC1 in unmodified control cells (Suppl. Fig. 3F). One cell line simultaneously expressing mGFP-EB1 and mCherry-PRC1 was selected for further studies (Suppl. Table 1).

N-terminally mGFP-tagged EB1 expressed from its endogenous locus tracked growing microtubule plus ends in interphase and mitosis (Suppl. Movie 3, Fig. 3A, B), as observed previously for over-expressed N-terminally tagged EB3[33] or C-terminally tagged EB1[47]. When we simultaneously imaged mGFP-EB1 and mCherry-PRC1 at different stages of mitosis, we noticed that the overall distribution of EB1 in the spindle was surprisingly similar to that of PRC1 (Fig. 3C, Suppl. Movie 4). Whereas EB1 localized more evenly throughout the spindle during metaphase (and also to the spindle poles as noted previously[49]), it started to accumulate more and more in the central spindle from anaphase on, showing a striking colocalization with PRC1. Midzone co-localization of EB1 with PRC1 after chromosomes started segregating was very evident in an average kymograph generated along the pole-to-pole spindle axis (Fig. 3D). Quantification of the normalized mGFP-EB1 and mCherry-PRC1 intensity in the spindle centre demonstrates a striking synchronous accumulation of EB1 and PRC1 in the central spindle during the later stages of mitosis (Fig. 3E).

Central spindle localization of EB1 depends on the presence of PRC1

To test whether EB1 localizes autonomously to the central spindle or whether this localization is PRC1-dependent, we knocked down PRC1 using siRNA in the RPE1 cells that

expressed mCherry-PRC1 and mGFP-EB1 from their endogenous locus (Fig. 4A). Spindles could still form after PRC1 knockdown, but were less organised and cells showed chromosome segregation effects, as observed before[15, 17, 59]. Whereas in control cells during metaphase mGFP-EB1 tracked astral microtubules and also localized prominently to microtubule bundles, in PRC1-depleted cells the bundle localization of EB1 was lost and it only tracked growing microtubule ends (Suppl. Movie 5, Fig. 4B). Even more strikingly, the pronounced central spindle localization of EB1 in anaphase was lost upon PRC1 depletion (Suppl. Movie 6, Fig. 4B, C). These results demonstrate that the localization of EB1 to central spindle bundles depends on the presence of PRC1.

An accessible C-terminal part of EB1 is required for central spindle localization

Several proteins known to interact with EB1, such as CLASPs and centralspindlin, also interact with PRC1 [39-42]. To test the hypothesis that EB1 may be recruited by these proteins to the central spindle in anaphase, we decided to examine the localization of EB1 carrying a C-terminal GFP tag in RPE1 cells. Fusing a fluorescent protein to the EB1 C-terminus interferes with the interaction with binding partners, particularly with CAP-Gly domains whose interaction with EB1 critically involves its C-terminal residue[38, 60]. To this end, we generated a hTERT-RPE1 cell line with endogenously expressed mCherry-PRC1 using CRISPR/Cas9-mediated gene editing (Suppl. Figs. 4A, B) and ectopically expressed EB1-GFP using lentiviral transduction. Western blot analysis demonstrated that again similar levels of mCherry-PRC1 were produced as untagged PRC1 in control cells (Suppl. Fig. 4C) and that 2-3 fold more EB1-GFP was expressed in the selected stable cell line than endogenous EB1 in control cells, hence showing mild EB1-GFP overexpression from the ectopic promotor (Suppl. Fig. 4D, Suppl. Table 1).

As expected, EB1-GFP tracked growing microtubule ends both in interphase and in mitosis (Fig. 5A, B). Simultaneous live cell imaging of mCherry-PRC1 and EB1-GFP at different mitotic stages showed no evident central spindle localization of EB1-GFP or any pronounced colocalization of EB1 with PRC1 (Suppl. Movie 7, Fig. 5C). An average kymograph generated along the spindle axis shows very clearly that mCherry-PRC1 started to strongly accumulate in the central spindle when chromosomes started segregating (Fig. 5C, D), as we observed before (Fig. 3D). This was in clear contrast to EB1-GFP whose localization decreased in the central spindle region over time (Fig. 5D, E). This result indicates that EB1 is recruited to the central spindle in mitosis via interactions involving its C-terminal part that can be blocked by fusing a fluorescent protein to the EB1 C-terminus.

EB1 turnover in the central spindle slows down as the midzone compacts

Plus end tracking EB1 has been shown to bind only transiently to growing microtubule ends, displaying fast binding/unbinding turnover[30-32, 34, 43]. To examine whether EB1 turnover is different when it is recruited to the central spindle, we performed FRAP analysis of mGFP-EB1 in gene-edited cells expressing mGFP-EB1 and mCherry-PRC1 at different stages of mitosis (Fig. 6A). Average intensity profiles of mGFP-EB1 (Fig. 6B) and average mGFP-

EB1 fluorescence recovery curves at the different stages of mitosis were generated from at least 8 individual bleached spindles per condition (except for telophase where 5 individual spindles were used) (Fig. 6C). We observed that the EB1 binding/unbinding turnover was significantly slower than at growing microtubule ends and further slowed down during mitosis. The recovery times for mGFP-EB1 were 2.1 ± 0.2 s, 3.1 ± 0.2 s, 7.0 ± 1 s, and 11 ± 2 s in metaphase, early anaphase, mid-anaphase, and late anaphase, respectively (Fig. 6D, E). There was no significant recovery of EB1 observed in telophase (Fig. 6C-E, Suppl. Movie 8). Remarkably, this means that EB1 showed the same trend of decreasing turnover in the central spindle as PRC1, even if EB1 turnover was a little more dynamic at all times. Consequently, the accumulation of EB1 increased over time in the central spindle during mitosis (Fig. 6B). As recovery slowed down during mitosis, the mobile fraction of mGFP-EB1 that recovered after photo-bleaching decreased concomitantly (Fig. 6E). Recovery times and mobile fractions of EB1 displayed a strikingly similar trend as those of PRC1 as mitosis proceeded (Fig. 6F). These data indicate a general slowdown of protein binding/unbinding turnover in the central spindle as it compacts during the course of mitosis.

A functional C-terminal tail of EB1 is important for cytokinesis

The absence of EB1 and its homolog EB3 has been shown previously to cause cytokinesis defects[42, 57, 58]. Given that we observed a central spindle localization of EB1 in addition to its microtubule end tracking behaviour in mGFP-EB1 expressing cells, we asked whether the interaction of EBs with central spindle proteins, possibly by reinforcing the structure of the central spindle in mitosis, is important for the cell to be able to correctly go through the later stages of mitosis. To this end, we selectively depleted endogenous EB1 and EB3 in the RPE1 cells expressing mCherry-PRC1 and C-terminally tagged EB1-GFP. After 24 h depletion, we observed the appearance of binucleated and multinucleated cells by fluorescence microscopy, indicating a cytokinesis defect (Suppl. Fig. 5A-C). The percentage of binucleated cells/multinucleated cells increased from 1.2 ± 0.3 % in control cells to 11 ± 3 % in cells expressing an EB1 that can track growing microtubule ends, but that cannot interact with its binding partners as a consequence of the C-terminal GFP fusion. These results suggest a function for the PRC1-dependent localization of EB1 to the central spindle in mitosis.

DISCUSSION

We measured the mitotic distribution and binding/unbinding dynamics of two major hub proteins of the cytoskeleton in live human cells, PRC1 and EB1. To ensure a situation that is as natural as possible, fluorescent fusion proteins were expressed from their endogenous loci in diploid RPE1 cells. We found that not only PRC1, but also EB1 localized to central spindle bundles and that the binding/unbinding turnover of both proteins strongly decreased from metaphase to telophase as the midzone compacted. This suggests that both proteins are

part of a solidifying interconnected protein network stabilizing the central spindle as mitosis proceeds.

Confirming previous observations either with immuno-stained fixed cells or with live cells in which fluorescently tagged PRC1 was overexpressed, we observed that PRC1 localized to extended microtubule bundles in the metaphase spindle, where it was recently shown to localize to microtubule bundles bridging sister kinetochore fibres[12, 13, 15, 19, 59]. From anaphase on, it strongly accumulated in the spindle midzone, as previously observed[14-19, 22, 27]. Since PRC1 is known to preferentially bind antiparallel microtubules[9-11], our data suggest that antiparallel microtubules exist throughout most of the metaphase spindle that then become focused in anaphase within ~ 5 min into short bundled antiparallel overlaps of ~ 1.7 µm length. The shape changes of the PRC1 profiles measured along the spindle axis over time reveal a process of longitudinal compaction, probably by a combination of motor-mediated microtubule sliding and microtubule stabilization in the midzone, and a pronounced reduction of binding/unbinding turnover of PRC1 over time.

The increasingly tighter binding of PRC1 could be due to an enhanced microtubule binding affinity when PRC1 becomes dephosphorylated at the transition from metaphase to anaphase, or due to protein trapping in compacting three-dimensional antiparallel overlaps consisting of multiple microtubules, or a combination of both factors. The similar slow-down in binding/unbinding turnover of EB1 indicates a general gradual solidification of the central spindle over mitosis time, probably involving multiple protein-protein interactions in interconnected networks of locally increasingly highly concentrated proteins. This local accumulation of microtubule associated proteins in turn then also slows down microtubule dynamics with their lifetimes increasing from tens of seconds to several minutes[2-6].

Recent in vitro reconstitution experiments with purified PRC1 and the kinesin KIF4A produced microtubule bundles with antiparallel overlaps by a 'bundle, slide and compaction' mechanism that had similar properties as the midzone bundles characterized here in living cells [61]. The kinetics of formation, the antiparallel overlap length and the low turnover of PRC1 in reconstituted minimal midzone bundles mimicked the physiological behaviour measured here, despite the absence of other prominent midzone proteins. This suggests that the activities present in the in vitro system, namely antiparallel microtubule bundling, antiparallel motor sliding, and protein compaction are key activities required for the formation of a basic midzone overlap architecture.

An interesting observation of our study is the striking PRC1-dependent colocalization of endogenously expressed and N-terminally tagged EB1 with PRC1 in microtubule bundles in the metaphase spindle and in the midzone of anaphase spindles. The EB1 orthologue Bim1 in budding yeast is well established to bind to the anaphase spindle depending on the PRC1 orthologue Ase1[28, 62]. Midzone localisation of EB1 has also been reported for Drosophila cells[53, 55]. However, for vertebrate cells, the situation has been less clear, because EB1 has often been reported to only track growing microtubule plus ends without showing any co-localization with PRC1, particularly when EB1 fusions with a fluorescent protein were

used[17, 45, 47, 48, 51], whereas immunofluorescence imaging showed midzone localization of EB1 in anaphase[54, 56].

Our data suggest that these difference may be due to the position of the fluorescent protein fused to EB1, because we observe colocalisation of EB1 with PRC1 only for N-terminally, but not C-terminally tagged EB1. Typically, EBs are well known to very transiently bind to microtubule ends and to dynamically recruit other proteins that interact with the EB1 C-terminus[30, 32, 37, 38], an interaction that can be disrupted by the presence of a fusion protein at the C-terminus[38, 60]. Because we observed that mGFP-EB1 with a freely accessible C-terminus became strongly bound to the central spindle, displaying increasingly slower binding/unbinding turnover, similar to PRC1, it is likely that in addition to recruiting other proteins to growing microtubule plus ends, EB1 may itself be recruited to PRC1-containing microtubule bundles via central spindle proteins that are part of both the PRC1 and EB1 protein interaction networks[39-42].

In this scenario, EB1 recruited to the central spindle could still contribute to microtubule binding, even if its affinity for the microtubule distant from the growing end is lower than for growing end binding[63]. A similar end-independent role of EB1 as a microtubule bridging factor within a larger protein network has been proposed for Golgi-microtubule connections[64]. Interconnecting both the EB1 and PRC1 protein interaction networks in the central spindle, is expected to lead to strong protein accumulations as a consequence of multiple local protein-protein interactions in this part of the cytoskeleton. This would explain the strikingly similar central bundle localizations and very slow binding dynamics of PRC1 and EB1 particularly at late mitotic stages. It could also provide an explanation for the reported role of EB1 for correct cytokinesis that depends on its ability to interact with other proteins via its C-terminus as our experiments showed[42, 57, 58].

In conclusion, we have quantified here morphological and dynamical properties of the central spindle during mitosis in gene-edited RPE1 cells using endogenously expressed fluorescent PRC1 and EB1 as reporters. Both proteins report a gradual compaction and solidification of the central spindle as mitosis proceeds, suggesting that central spindle stability is achieved by interconnecting two major protein interaction networks of the microtubule cytoskeleton, particularly in late mitosis. The previous observation of the EB1 orthologue Bim1 being recruited by the PRC1 orthologue Ase1 to the budding yeast spindle, and the slowing down binding/unbinding turnover of Ase1 in the same organism in anaphase may suggest that the interaction between these EB1 and PRC1 protein networks during late mitosis is evolutionarily conserved to stabilize a shortening central spindle[28, 62].

METHODS

Donor vector constructs, guide RNA design and cloning: To generate human telomerase reverse transcriptase-immortalized retinal pigmented epithelium (hTERT-RPE1) cell lines expressing fluorescently tagged PRC1 and/or EB1 from their endogenous locus, we used

CRISPR/Cas9-mediated gene editing to fuse mGFP or mCherry sequences to the PRC1 and/or EB1 genes[65, 66]. Homology arms of the donor vectors were made from genomic DNA of hTERT-RPE1 cells by PCR amplification of the flanking regions (1.2 kb each) of the PRC1 and EB1 genes. The coding sequences of mGFP and mCherry were PCR amplified from plasmids. Then the homology arms and fluorescent protein sequences were assembled and cloned into the BamHI site of a pUC19 vector using Gibson assembly (Clontech). The primer sequences for the mGFP-EB1, mGFP-PRC1 and mCherry-PRC1 donor constructs are listed in Suppl. Material 1 and 2. The reverse primers for the generation of the donor constructs encoded also a sequence encoding a five-glycine linker sequence to be inserted between mGFP or mCherry and PRC1 or the sequence AQAGGSGGAGSGGEGAVDG to be inserted between mGFP and EB1 (Suppl. Material 1 and 2). The latter linker is identical to the previously used linker in a GFP-EB3 construct that was overexpressed in human cells[33]. The protospacer adjacent motifs (PAM) in the donor plasmids were modified to silent mutations by site directed mutagenesis to ensure that the donor plasmids are not cleaved by Cas9 nuclease.

Guide RNA (gRNA) sequences specifying the site of Cas9 cleavage in endogenous DNA were designed from the genomic EB1 and PRC1 sequences using the guide RNA design resource (http://crispr.mit.edu/) selecting the top gRNA hits (Suppl. Material 1 and 2). Each guide RNA pair was cloned into either the 'All-in-one-mCherry' plasmid (AIO-mCherry, gift from Steve Jackson (Addgene plasmid # 74120; http://n2t.net/addgene:74120; RRID: Addgene_74120)) or into 'All-in-one-GFP' plasmid (AIO-GFP, gift from Steve Jackson (Addgene plasmid # 74119 http://n2t.net/addgene:74119; RRID: Addgene_74119))[65]. The AIO plasmids also expresses Cas9 nickase.

CRISPR/Cas9-mediated gene editing: hTERT-RPE1 cells were cultured at 37°C and 10% CO_2 in Dulbecco's Modified Eagle Medium (DMEM) supplemented with 10% fetal bovine serum, 1 x non-essential amino acids (Thermofisher Scientific) and 1x penicillin-streptomycin (Thermofisher Scientific). hTERT-RPE1 cells were transfected with donor plasmid and AIO plasmid with the appropriate gRNAs using a Neon transfection system (Thermofisher Scientific). For 5 x 10^6 cells, 5 µg of donor plasmid and 5 µg of gRNA plasmids were used for transfection (1050 V pulse voltage, 35 ms pulse width, and pulse number 2). After 16-18 hours, cells were selected by flow cytometry on the basis of expression of the fluorescence protein marker of the AIO plasmid. The selected cells were pooled and after two weeks of cell growth, flow cytometry was performed again, this time based on fluorescent protein expression of the edited endogenous genes, to collect single cells in 96 well plates. After 2 - 3 weeks when the cells became confluent, the monoclonal cultures were transferred to 24 well plates. A minimum of 30 clones per cell line to be generated were selected at this stage for further analysis. Genomic DNA was extracted and a genotypic characterization of the single cell clones was performed to verify the correct locus insertion and to determine the number of modified alleles. Primers pairs (Suppl. Material 1 and 2) consisting of one primer that binds outside of one of the homology arms in the genomic region and another primer that binds inside either the mGFP or mCherry sequence were used

to verify insertion into the correct locus. Primer pairs (Suppl. Material 1 and 2) consisting of one primer that binds in the genomic region just outside of one of the homology arms and the other primer that binds inside the other homology arm, were used to detect the number of modified alleles. One hTERT-RPE1 cell clone expressing mGFP-EB1 was further edited to express also endogenous mCherry-PRC1. The CRISPR/Cas9 gene-edited cell lines were further characterized by determining protein expression levels of the individual clones by western blotting.

Lentivirus-mediated stable cell line development: The EB1-GFP lentivirus expression construct was made by PCR amplification of EB1-GFP from pEGFP N1 EB1-GFP (JB131) (gift from Tim Mitchison & Jennifer Tirnauer (Addgene plasmid # 39299; http://n2t.net/addgene:39299; RRID: Addgene_39299) followed by cloning into a pLVX-puro vector (Clontech) using the XhoI and BamHI restriction sites (primers in Suppl. Material 2). EB1-GFP expressing lentivirus particles were generated by transfecting *psPAX2*, *pMD2.G* (helper plasmids), and pLVX-puro-EB1-GFP plasmids in 293FT cells. hTERT-RPE1 cells already expressing endogenous mCherry-PRC1 were transduced using the EB1-GFP lentivirus particles. hTERT-RPE1 cells stably expressing EB1 with a C-terminal GFP fusion from a randomly inserted ectopic EB1-GFP gene under the control of a CMV promoter were selected on puromycin (10 µg/ml) for 3 - 4 days. Cells expressing low levels of EB1-GFP were selected by flow cytometry and were used for live cell imaging. The expression levels were determined by western blot using EB1 monoclonal antibodies.

siRNA transfection: hTERT-RPE1 wild type cells and cells coexpressing mGFP-EB1 and mCherry-PRC1 were seeded at a density of 0.2 x 10^6 cells/ml. After one day, cells coexpressing mGFP-EB1 and mCherry-PRC1 cells were transfected either with 200 nM of non-targeting siRNA or siRNA against PRC1. Lipofectamine RNAimax was used as a transfection reagent. The degree of protein depletion was analysed and quantified by western blot. For studying the effect of EB1/EB3 depletion on cytokinesis, ectopically expressing EB1-GFP and endogenous mCherry-PRC1coexpressing cells were seeded at a density of 0.2 x 10^6 cells/ml. After one day, cells were either transfected with 200 nM of non-targeting siRNA or siRNA against both EB1 and EB3. Lipofectamine RNAimax was used as a transfection reagent. At the time of siRNA transfection, cells were also treated with 2.5 mM thymidine and incubated for 16-18 hours to block the cells at the G1/S transition and 8 hours before live cell imaging, cells were washed several times with 1 x PBS and once with culture medium. (The time of imaging coincides with 24 hours after siRNA transfection).

Live cell imaging: Cells were seeded at a density of 0.5 x 10^5 cells/ml and six hours later thymidine was added at a final concentration of 2.5 mM to block the cells at the G1/S transition. After 16-18 hours incubation, cells were washed several times with 1x PBS and once with the culture medium. After washing, cells were seeded with fresh culture medium in 2-well dishes (ibidi) and kept in the CO_2 incubator at 37°C for 8-10 hours to allow the cells to release from at the G1/S transition and enter mitosis. Before imaging the DMEM medium was replaced with DMEM without phenol red, supplemented with 25 mM HEPES (pH 7.6) buffer. For the visualization of DNA, the live cell dye Hoechst 33342 was added. The cells in

mitosis were imaged at 37°C by spinning disk confocal microscopy on a Zeiss Axio Observer Z1 equipped with a Yokogawa CSU M1 spinning disk unit, a FRAP unit and Prime 95B sCMOS camera (3i, London, UK). Time lapse imaging over the entire duration of mitosis was performed in three different z-planes separated by 0.5 µm using a 63 x oil objective at 2 frames per minute and exposure times of 100 ms for mGFP-PRC1 imaging (488 nm) and 40 ms for Hoechst-stained DNA imaging (405 nm). For fluorescence recovery after photobleaching (FRAP) of either mGFP-PRC1 or mGFP-EB1, a small area (with 0.6 µm diameter for mGFP-PRC1 or 0.63 µm for mGFP-EB1) in the microtubule overlap region was bleached using the 488 nm laser. Images were recorded in three different z-planes separated by 0.5 µm at 30 frames per minute over a period of 3 min post bleaching. FRAP experiments of mGFP-PRC1 and mGFP-EB1 were performed using a 63 x oil and 100 x oil objective, respectively. Time lapse imaging of mGFP-EB1 and mCherry-PRC1 co-expressing cells was performed in a single z-plane using a 100 x oil objective at 1 frame per second at exposure times of 50 ms (488 nm) and 30 ms (405 nm and 640 nm) over a period of 10 - 15 min. Time lapse imaging of cells expressing ectopic EB1-GFP and endogenous mCherry-PRC1 after selective depletion of both endogenous EB1 and EB3 was performed using a Nikon Eclipse Ti2 microscope equipped with spinning disk unit using 100 x oil objective at 1 frame per second and exposure times of 50 ms (488 nm) and 30 ms (405 nm). The effect of EB1/EB3 depletion on cytokinesis was quantitated by counting the number of binucleated/multinucleated cells. A minimum of 500 cells were counted for control and EB depleted cells each, the experiment was performed three times. The kymograph of a metaphase cell ectopically expressing EB1-GFP (Fig. 5B) was generated from a movie, imaged at 4 frames per second using a 100 x oil objective and exposure times of 50 ms (488 nm).

Determination of protein expression levels: Commercial antibodies were used to check the expression levels of proteins by western blot of cell lysate. EB1 and PRC1 proteins were detected by using antibodies sc-47704 and sc-377544 (both Santa Cruz Biotechnlogy), respectively. Tubulin was used as a loading control and detected using antibody ab18251 (Abcam). For detection of these primary antibodies, horse raddish peroxidase-coupled secondary antibodies were used.

Average kymograph generation: For each cell of interest, a manual tracking procedure was used to align the cell: for each frame the position of each centrosome was marked manually; the image was then translated and rotated to centre the midzone and align the spindle with the horizontal image axis. A kymograph was then automatically generated along the centrosomal axis averaging over a line width of 8 µm. Kymographs generated from individual cells were averaged together: for each kymograph the space (x) axis was normalized to the average metaphase centrosome distance, and the time (y) axis was shifted to align the start of anaphase, based on the DNA channel. For each fluorescence channel, a fluorescence profile of the average intensity in the midzone region was produced from the average kymograph for further analysis.

Average fluorescence kymograph analysis: To extract the time course of the total PRC1 profile width (a measure for spindle length), the central PRC1 peak width (a measure of antiparallel overlap length), and the distance between separating chromosomes for Fig. 1D, the mathematical functions were used for fits to background-subtracted and bleaching-corrected intensity profiles (using OriginLab): A single Gaussian distribution was found to fit well metaphase PRC1 profiles, allowing to quantify its full width at half maximum (FWHM), i.e. the metaphase spindle length as labelled by PRC1. A sum of one central Gaussian peak with two equidistant side Gaussian peaks with identical heights and widths was used to fit anaphase PRC1 profiles; this allowed to quantify (i) the width of the entire profile (defined as the distance between the side peaks plus one FWHM of the side peaks) and (ii) the FWHM of the central PRC1 peak (could be determined reliably from t = 3 min onwards). A sum of 2 spatially displaced and otherwise identical Gaussian distributions was fit to the anaphase DNA profiles to extract the average distance between separating chromosomes. The maximum peak intensity was extracted from the PRC1 profiles by averaging the neighbouring 5 intensity values around the maximum value in each profile.

To visualise the time course of the PRC1 and EB1 intensities in the spindle centre (and the central DNA intensity as a control) for Fig. 3E and 5E, their intensities were plotted from a 1 µm wide region along central line of the average kymographs (corresponding to an 8 µm x 1 µm region in the cell midzone) where the PRC1 and EB1 intensities peaked in late mitosis.

FRAP analysis: Images were corrected for drift and centered by manually tracking centrosomes, as described above. A 20 µm long, 80 pixel wide (8 µm) line was drawn along the centrosomal axis. The PRC1/DNA intensity profile was generated along the centrosomal axis at the time point before FRAP. The background intensity was subtracted and the intensity profile normalized to the maximum value. In the FRAP movie, the intensity was measured at the FRAP point (~0.6 µm radius circle) at every time point and normalized to the average intensity of 4 time points before FRAP. FRAP intensity curves from individual movies were classified into metaphase to telophase stage using the estimated time since mitosis and further refined using the PRC1/DNA intensity profiles. All FRAP intensity data for a specific phase were averaged together and fit with a FRAP recovery curve $I = I_0 + I_a(1-e^{-t/\tau})$ (Fig. 2D and Fig 6D) to obtain the recovery time τ, and the mobile fraction $I_a/(1-I_0)$ (Fig. 2E and 6E).

Time stack to visualize EB1 end tracking in interphase cells: The colour-coded time-stack images in Fig. 3A and 5A were generated using a previously developed ImageJ macro [67]. Each individual frame of 20 time-lapse images acquired at 1s interval were colour-coded from red to blue sequentially in accordance to the rainbow order. Subsequently, the colour-coded time-lapse images were stacked using the z-stack option in ImageJ.

ACKNOWLEDGEMENTS

We thank the Flow Cytometry, the Cell Services and the Advanced Light Microscopy science technology platforms of the Francis Crick Institute for cell sorting, for providing wild-type hTERT-RPE1 and 293FT cells, and for help with some of the confocal microscopy imaging, respectively. We thank Stephen P. Jackson, Jennifer Tirnauer and Tim Mitchison for providing plasmids. We thank Julian Gannon for help with cell culture.

FUNDING

This work was supported by the Francis Crick Institute, which receives its core funding from Cancer Research UK (FC001163), the UK Medical Research Council (FC001163), and the Wellcome Trust (FC001163). T.S. acknowledges support from the European Research Council (Advanced Grant, project 323042). J.A., W.M.L., and T.S. acknowledge also the support of the Spanish Ministry of Economy, Industry and Competitiveness to the CRG-EMBL partnership, the Centro de Excelencia Severo Ochoa and the CERCA Programme of the Generalitat de Catalunya.

AUTHOR CONTRIBUTIONS

J.A.: Conceptualization, cell lines development, experiments, data analysis, writing of the manuscript, figure preparation. **N.I.C.**: Microscopy support, data analysis, figure preparation. **W.M.L.**: Help with cell line development and figure preparation. **T.S.**: Conceptualization, data analysis, writing of the manuscript, supervision, funding.

LITERATURE

1. Meraldi, P., Draviam, V.M. & Sorger, P.K. Timing and checkpoints in the regulation of mitotic progression. *Dev Cell* **7**, 45-60 (2004).
2. Needleman, D.J. *et al.* Fast microtubule dynamics in meiotic spindles measured by single molecule imaging: evidence that the spindle environment does not stabilize microtubules. *Mol Biol Cell* **21**, 323-333 (2010).
3. Saxton, W.M. & McIntosh, J.R. Interzone microtubule behavior in late anaphase and telophase spindles. *J Cell Biol* **105**, 875-886 (1987).
4. Saxton, W.M. *et al.* Tubulin dynamics in cultured mammalian cells. *J Cell Biol* **99**, 2175-2186 (1984).
5. Zhai, Y., Kronebusch, P.J., Simon, P.M. & Borisy, G.G. Microtubule dynamics at the G2/M transition: abrupt breakdown of cytoplasmic microtubules at nuclear envelope breakdown and implications for spindle morphogenesis. *J Cell Biol* **135**, 201-214 (1996).
6. Mitchison, T.J. & Salmon, E.D. Poleward kinetochore fiber movement occurs during both metaphase and anaphase-A in newt lung cell mitosis. *J Cell Biol* **119**, 569-582 (1992).

7. Glotzer, M. The 3Ms of central spindle assembly: microtubules, motors and MAPs. *Nat Rev Mol Cell Biol* **10**, 9-20 (2009).
8. Green, R.A., Paluch, E. & Oegema, K. Cytokinesis in animal cells. *Annu Rev Cell Dev Biol* **28**, 29-58 (2012).
9. Bieling, P., Telley, I.A. & Surrey, T. A minimal midzone protein module controls formation and length of antiparallel microtubule overlaps. *Cell* **142**, 420-432 (2010).
10. Janson, M.E. *et al.* Crosslinkers and motors organize dynamic microtubules to form stable bipolar arrays in fission yeast. *Cell* **128**, 357-368 (2007).
11. Subramanian, R. *et al.* Insights into antiparallel microtubule crosslinking by PRC1, a conserved nonmotor microtubule binding protein. *Cell* **142**, 433-443 (2010).
12. Kajtez, J. *et al.* Overlap microtubules link sister k-fibres and balance the forces on bi-oriented kinetochores. *Nat Commun* **7**, 10298 (2016).
13. Polak, B., Risteski, P., Lesjak, S. & Tolic, I.M. PRC1-labeled microtubule bundles and kinetochore pairs show one-to-one association in metaphase. *EMBO Rep* **18**, 217-230 (2017).
14. Nunes Bastos, R. *et al.* Aurora B suppresses microtubule dynamics and limits central spindle size by locally activating KIF4A. *J Cell Biol* **202**, 605-621 (2013).
15. Mollinari, C. *et al.* PRC1 is a microtubule binding and bundling protein essential to maintain the mitotic spindle midzone. *J Cell Biol* **157**, 1175-1186 (2002).
16. Cundell, M.J. *et al.* The BEG (PP2A-B55/ENSA/Greatwall) pathway ensures cytokinesis follows chromosome separation. *Mol Cell* **52**, 393-405 (2013).
17. Pamula, M.C. *et al.* High-resolution imaging reveals how the spindle midzone impacts chromosome movement. *J Cell Biol* **218**, 2529-2544 (2019).
18. Hu, C.K., Ozlu, N., Coughlin, M., Steen, J.J. & Mitchison, T.J. Plk1 Negatively Regulates PRC1 to Prevent Premature Midzone Formation before Cytokinesis. *Mol Biol Cell* (2012).
19. Neef, R. *et al.* Choice of Plk1 docking partners during mitosis and cytokinesis is controlled by the activation state of Cdk1. *Nat Cell Biol* **9**, 436-444 (2007).
20. Jiang, W. *et al.* PRC1: a human mitotic spindle-associated CDK substrate protein required for cytokinesis. *Mol Cell* **2**, 877-885 (1998).
21. Kurasawa, Y., Earnshaw, W.C., Mochizuki, Y., Dohmae, N. & Todokoro, K. Essential roles of KIF4 and its binding partner PRC1 in organized central spindle midzone formation. *EMBO J* **23**, 3237-3248 (2004).
22. Zhu, C. & Jiang, W. Cell cycle-dependent translocation of PRC1 on the spindle by Kif4 is essential for midzone formation and cytokinesis. *Proc Natl Acad Sci U S A* **102**, 343-348 (2005).
23. Duellberg, C., Fourniol, F.J., Maurer, S.P., Roostalu, J. & Surrey, T. End-binding proteins and Ase1/PRC1 define local functionality of structurally distinct parts of the microtubule cytoskeleton. *Trends Cell Biol* **23**, 54-63 (2013).
24. Mishima, M. Centralspindlin in Rappaport's cleavage signaling. *Semin Cell Dev Biol* **53**, 45-56 (2016).
25. Roostalu, J., Schiebel, E. & Khmelinskii, A. Cell cycle control of spindle elongation. *Cell Cycle* **9**, 1084-1090 (2010).
26. Mastronarde, D.N., McDonald, K.L., Ding, R. & McIntosh, J.R. Interpolar spindle microtubules in PTK cells. *J Cell Biol* **123**, 1475-1489 (1993).
27. Cundell, M.J. *et al.* A PP2A-B55 recognition signal controls substrate dephosphorylation kinetics during mitotic exit. *J Cell Biol* **214**, 539-554 (2016).

28. Khmelinskii, A., Roostalu, J., Roque, H., Antony, C. & Schiebel, E. Phosphorylation-dependent protein interactions at the spindle midzone mediate cell cycle regulation of spindle elongation. *Dev Cell* **17**, 244-256 (2009).
29. Akhmanova, A. & Steinmetz, M.O. Control of microtubule organization and dynamics: two ends in the limelight. *Nat Rev Mol Cell Biol* **16**, 711-726 (2015).
30. Bieling, P. *et al.* CLIP-170 tracks growing microtubule ends by dynamically recognizing composite EB1/tubulin-binding sites. *J Cell Biol* **183**, 1223-1233 (2008).
31. Bieling, P. *et al.* Reconstitution of a microtubule plus-end tracking system in vitro. *Nature* **450**, 1100-1105 (2007).
32. Dixit, R. *et al.* Microtubule plus-end tracking by CLIP-170 requires EB1. *Proc Natl Acad Sci U S A* **106**, 492-497 (2009).
33. Komarova, Y. *et al.* Mammalian end binding proteins control persistent microtubule growth. *J Cell Biol* **184**, 691-706 (2009).
34. Roostalu, J. *et al.* The speed of GTP hydrolysis determines GTP cap size and controls microtubule stability. *Elife* **9** (2020).
35. Maurer, S.P., Fourniol, F.J., Bohner, G., Moores, C.A. & Surrey, T. EBs recognize a nucleotide-dependent structural cap at growing microtubule ends. *Cell* **149**, 371-382 (2012).
36. Zhang, R., Alushin, G.M., Brown, A. & Nogales, E. Mechanistic Origin of Microtubule Dynamic Instability and Its Modulation by EB Proteins. *Cell* **162**, 849-859 (2015).
37. Honnappa, S. *et al.* An EB1-binding motif acts as a microtubule tip localization signal. *Cell* **138**, 366-376 (2009).
38. Honnappa, S. *et al.* Key interaction modes of dynamic +TIP networks. *Mol Cell* **23**, 663-671 (2006).
39. Lee, K.Y., Esmaeili, B., Zealley, B. & Mishima, M. Direct interaction between centralspindlin and PRC1 reinforces mechanical resilience of the central spindle. *Nat Commun* **6**, 7290 (2015).
40. Liu, J. *et al.* PRC1 cooperates with CLASP1 to organize central spindle plasticity in mitosis. *J Biol Chem* **284**, 23059-23071 (2009).
41. Mimori-Kiyosue, Y. *et al.* CLASP1 and CLASP2 bind to EB1 and regulate microtubule plus-end dynamics at the cell cortex. *J Cell Biol* **168**, 141-153 (2005).
42. Verma, V. & Maresca, T.J. Microtubule plus-ends act as physical signaling hubs to activate RhoA during cytokinesis. *Elife* **8** (2019).
43. Roth, D., Fitton, B.P., Chmel, N.P., Wasiluk, N. & Straube, A. Spatial positioning of EB family proteins at microtubule tips involves distinct nucleotide-dependent binding properties. *J Cell Sci* **132** (2018).
44. Applegate, K.T. *et al.* plusTipTracker: Quantitative image analysis software for the measurement of microtubule dynamics. *J Struct Biol* **176**, 168-184 (2011).
45. Chen, B.C. *et al.* Lattice light-sheet microscopy: imaging molecules to embryos at high spatiotemporal resolution. *Science* **346**, 1257998 (2014).
46. Matov, A. *et al.* Analysis of microtubule dynamic instability using a plus-end growth marker. *Nat Methods* **7**, 761-768 (2010).
47. Mimori-Kiyosue, Y., Shiina, N. & Tsukita, S. The dynamic behavior of the APC-binding protein EB1 on the distal ends of microtubules. *Curr Biol* **10**, 865-868 (2000).
48. Piehl, M., Tulu, U.S., Wadsworth, P. & Cassimeris, L. Centrosome maturation: measurement of microtubule nucleation throughout the cell cycle by using GFP-tagged EB1. *Proc Natl Acad Sci U S A* **101**, 1584-1588 (2004).

49. Tirnauer, J.S., Canman, J.C., Salmon, E.D. & Mitchison, T.J. EB1 targets to kinetochores with attached, polymerizing microtubules. *Mol Biol Cell* **13**, 4308-4316 (2002).
50. Tirnauer, J.S., Salmon, E.D. & Mitchison, T.J. Microtubule plus-end dynamics in Xenopus egg extract spindles. *Mol Biol Cell* **15**, 1776-1784 (2004).
51. Yamashita, N. *et al.* Three-dimensional tracking of plus-tips by lattice light-sheet microscopy permits the quantification of microtubule growth trajectories within the mitotic apparatus. *J Biomed Opt* **20**, 101206 (2015).
52. Beinhauer, J.D., Hagan, I.M., Hegemann, J.H. & Fleig, U. Mal3, the fission yeast homologue of the human APC-interacting protein EB-1 is required for microtubule integrity and the maintenance of cell form. *J Cell Biol* **139**, 717-728 (1997).
53. de Lartigue, J., Brust-Mascher, I. & Scholey, J.M. Anaphase B spindle dynamics in Drosophila S2 cells: Comparison with embryo spindles. *Cell Div* **6**, 8 (2011).
54. Morrison, E.E., Wardleworth, B.N., Askham, J.M., Markham, A.F. & Meredith, D.M. EB1, a protein which interacts with the APC tumour suppressor, is associated with the microtubule cytoskeleton throughout the cell cycle. *Oncogene* **17**, 3471-3477 (1998).
55. Rogers, S.L., Rogers, G.C., Sharp, D.J. & Vale, R.D. Drosophila EB1 is important for proper assembly, dynamics, and positioning of the mitotic spindle. *J Cell Biol* **158**, 873-884 (2002).
56. Sun, L. *et al.* EB1 promotes Aurora-B kinase activity through blocking its inactivation by protein phosphatase 2A. *Proc Natl Acad Sci U S A* **105**, 7153-7158 (2008).
57. Ferreira, J.G., Pereira, A.J., Akhmanova, A. & Maiato, H. Aurora B spatially regulates EB3 phosphorylation to coordinate daughter cell adhesion with cytokinesis. *J Cell Biol* **201**, 709-724 (2013).
58. Strickland, L.I., Wen, Y., Gundersen, G.G. & Burgess, D.R. Interaction between EB1 and p150glued is required for anaphase astral microtubule elongation and stimulation of cytokinesis. *Curr Biol* **15**, 2249-2255 (2005).
59. Zhu, C., Lau, E., Schwarzenbacher, R., Bossy-Wetzel, E. & Jiang, W. Spatiotemporal control of spindle midzone formation by PRC1 in human cells. *Proc Natl Acad Sci U S A* **103**, 6196-6201 (2006).
60. Skube, S.B., Chaverri, J.M. & Goodson, H.V. Effect of GFP tags on the localization of EB1 and EB1 fragments in vivo. *Cytoskeleton (Hoboken)* **67**, 1-12 (2010).
61. Hannabuss, J. *et al.* Self-Organization of Minimal Anaphase Spindle Midzone Bundles. *Curr Biol* **29**, 2120-2130 e2127 (2019).
62. Khmelinskii, A., Lawrence, C., Roostalu, J. & Schiebel, E. Cdc14-regulated midzone assembly controls anaphase B. *J Cell Biol* **177**, 981-993 (2007).
63. Maurer, S.P., Bieling, P., Cope, J., Hoenger, A. & Surrey, T. GTPgammaS microtubules mimic the growing microtubule end structure recognized by end-binding proteins (EBs). *Proc Natl Acad Sci U S A* **108**, 3988-3993 (2011).
64. Yang, C. *et al.* EB1 and EB3 regulate microtubule minus end organization and Golgi morphology. *J Cell Biol* **216**, 3179-3198 (2017).
65. Chiang, T.W., le Sage, C., Larrieu, D., Demir, M. & Jackson, S.P. CRISPR-Cas9(D10A) nickase-based genotypic and phenotypic screening to enhance genome editing. *Sci Rep* **6**, 24356 (2016).
66. Koch, B. *et al.* Generation and validation of homozygous fluorescent knock-in cells using CRISPR-Cas9 genome editing. *Nat Protoc* **13**, 1465-1487 (2018).

67. Uenoyama, A. & Miyata, M. Gliding ghosts of Mycoplasma mobile. *Proc Natl Acad Sci U S A* **102**, 12754-12758 (2005).

FIGURE LEGENDS

Figure 1. Live cell imaging of endogenously expressed mGFP-PRC1 during mitosis.
(A) Spinning disk confocal microscopy of endogenous mGFP-PRC1 (green) and Hoechst-stained chromosomes (blue) in gene-edited RPE1 cells. Images were acquired every 30 seconds from the start of mitosis to telophase. Representative examples are shown for the different phases of mitosis as identified by the chromosome position and central spindle appearance. Scale bar = 10 µm**.** Time is in min:s. See also Movie S1. **(B)** Individual kymographs (space-time-plots) along the spindle pole-to-pole axis, were generated from whole mitosis movies for mGFP-PRC1 (green) and Hoechst-stained chromosomes (blue). The top image displays a pro-metaphase cell. An average kymograph was generated from 17 individual kymographs (Methods). **(C)** Example mGFP-PRC1 (left) and DNA (right) intensity profiles as extracted from the average kymograph. Profiles with error bars are shown in Suppl. Fig. 2B. **(D)** Time courses of total PRC1 profile width, PRC1 central peak width and maximum intensity as a function of time (from -3.0 to 11.5 minutes) as extracted from fits to the average mGFP-PRC1 intensity profiles, and of the chromosome separation distance as extracted from fits to the DNA intensity profiles (see Methods). The green line is a fit to the PRC1 central peak width data using a monoexponential decay function. Error bars indicate the standard error either as obtained directly from the fits to the intensity profiles or for derived parameters after error propagation.

Figure 2. FRAP analysis of PRC1 turnover during mitosis.
(A) Analysis of mGFP-PRC1 binding/unbinding turnover in the central spindle of gene-edited RPE1 cells at different stages of mitosis. The position of Hoechst-stained chromosomes (top row) and the binding pattern of PRC1 to the spindle (second row) were used to identify the mitotic stages. For each stage, mGFP-PRC1 bound to the spindle is shown just before the photo-bleach (pre-bleach, second row), at the time of bleaching a circular area with ~ 0.6 µm radius (bleach, third row) and 12 s after the bleach mark was set (12 s post-bleach, bottom row). The position of the photo-bleached area is indicated by the white arrow heads. Scale bar = 10 µm. Time is in min:s. See also Movie S2. **(B)** Normalized average PRC1 (dark green) and chromosome (dark blue) intensity profiles along the spindle pole-to-pole axis at the time just before photo-bleaching. **(C)** Average fluorescence recovery curves (black symbols are average intensities, $n \geq 12$ for each condition) at the different stages of mitosis shown in (A). Error bars are standard deviation. **(D)** Comparison of the fluorescence recovery curves from (B) here in a single graph. Error bars are standard error. **(E)** The mobile fraction and the recovery time of mGFP-PRC1 after photobleaching at different times during mitosis. Error bars are standard error.

Figure 3. Live cell imaging of endogenously expressed mGFP-EB1 and mCherry-PRC1 during mitosis.

(A, B) Spinning disk confocal microscopy of endogenous mGFP-EB1 in RPE1 cells (also expressing mCherry-PRC1). **(A)** Image of an interphase cell (left) and a time stack from a time lapse movie of the same cell (right) showing EB1 microtubule end tracking traces in false colors. See also Movie S3. **(B)** Image of a metaphase cell (left) and a kymograph from a time lapse movie of the same cell (right) showing EB1 tracks on astral and some tracks on spindle microtubules. **(C)** Confocal microscopy images of gene-edited RPE1 cells co-expressing mGFP-EB1 (green) and mCherry-PRC1 (magenta) from their endogenous locus. Chromosomes are stained by Hoechst (blue). Images were acquired every second from metaphase to telophase. Time is in min:s. See also Movie S4. **(D)** Average kymograph generated from 14 movies along the spindle pole-to-pole axis. The individual fluorescence channels for chromosomes (blue), EB1 (green) and PRC1 (magenta) are shown under a representative metaphase spindle image with these channels. **(E)** Average fluorescence intensity of mGFP-EB1 (green), and mCherry-PRC1 (magenta) and Hoechst-stained DNA (blue) in the central spindle (along the dashed line in D) as function of the time of mitosis.

Figure 4. Depletion of PRC1 abolishes the localization of mGFP-EB1 to the central spindle.

(A) Western blot showing depletion of PRC1 in RPE1 cells expressing mGFP-EB1 and mCherry PRC1 from their endogenous locus. The mCherry PRC1 and mGFP-EB1 coexpressing cells were treated either with non-targeting siRNA (siControl) or siRNA targeting the PRC1. Tubulin was used as a loading control. **(B)** Confocal microscopy images of mGFP-EB1 (green) and mCherry-PRC1 (magenta) expressed from their endogenous locus in living RPE1 cells during metaphase and anaphase. Cells were treated with either control siRNA (siControl) or PRC1 siRNA (siPRC1). Chromosomes are stained with Hoechst (blue). See also Movies S5 and S6. **(C)** Merged and individual kymographs generated along the spindle pole-to-pole axis from metaphase and anaphase movies showing the localizations of mGFP-EB1 (green), mCherry-PRC1 (magenta) and DNA (blue) in control and PRC1-depleted cells.

Figure 5. Ectopically expressed EB1 with a C-terminal GFP does not co-localize with PRC1.

(A, B) Spinning disk confocal microscopy of ectopically expressed EB1-GFP in interphase and metaphase cells. **(A)** Image of an interphase cell (left) and a time stack from a time lapse movie of the same cell (right) showing EB1-GFP microtubule end tracking traces. **(B)** Image of a metaphase cell (left) and a kymograph along the spindle axis of the same cell (right) showing EB1-GFP tracking astral microtubule ends. **(C)** Confocal microscopy images of ectopically expressed EB1-GFP (green) and mCherry-PRC1 (magenta) expressed from its endogenous locus during different stages of mitosis in living RPE1 cells. Chromosomes are stained by Hoechst (blue). Images were acquired every second from metaphase to telophase.

Time is in min:s. See also Movie S7. **(D)** Average kymograph generated along the spindle pole-to-pole axis from 14 mitotic movies. **(E)** Average fluorescence intensity of EB1-GFP, mCherry-PRC1 and DNA in the central spindle (along the dashed line in D) as function of the time of mitosis.

Figure 6. FRAP analysis of mGFP-EB1 turnover during mitosis.

(A) Analysis of the EB1 binding/unbinding turnover in the central spindle of gene-edited RPE1 cells expressing mGFP-EB1 (green) and mCherry-PRC1 (magenta) from their endogenous loci. For each mitotic stage shown, mGFP-EB1 bound to the spindle is shown just before the bleach (pre-bleach, top row), at the time of bleaching a circular area with a ~0.63 µm radius (bleach, second row) and 12 s after the bleach mark was set (12 s post-bleach, bottom row). The position of the photobleached area is indicated by the white arrow heads. See also Movie S8. **(B)** Normalized average mGFP-EB1 (dark green) intensity profiles along the spindle pole-to-pole axis at a time just before photo-bleaching. **(C)** Average mGFP-EB1 fluorescence recovery time courses (black symbols, $n \geq 8$ for each condition except for telophase where $n = 5$) at the different stages of mitosis shown in (A, bottom row). The error bars are standard deviation. **(D)** Comparison of the fluorescence recovery curves of mGFP-EB1 from (B) in a single graph. Error bars are standard error. **(E)** The mobile fraction and the recovery time of mGFP-EB1 after photo-bleaching at different times during mitosis. Error bars are standard error. **(F)** Comparison of the recovery times (top) and mobile fractions (bottom) of mGFP-EB1 (green circles) and mGFP-PRC1 (red squares) as a function of overlap length. Inset: PRC1 overlap length and EB1 localization length as extracted from fits to the respective intensity profiles. Error bars are standard error.

Figure 1

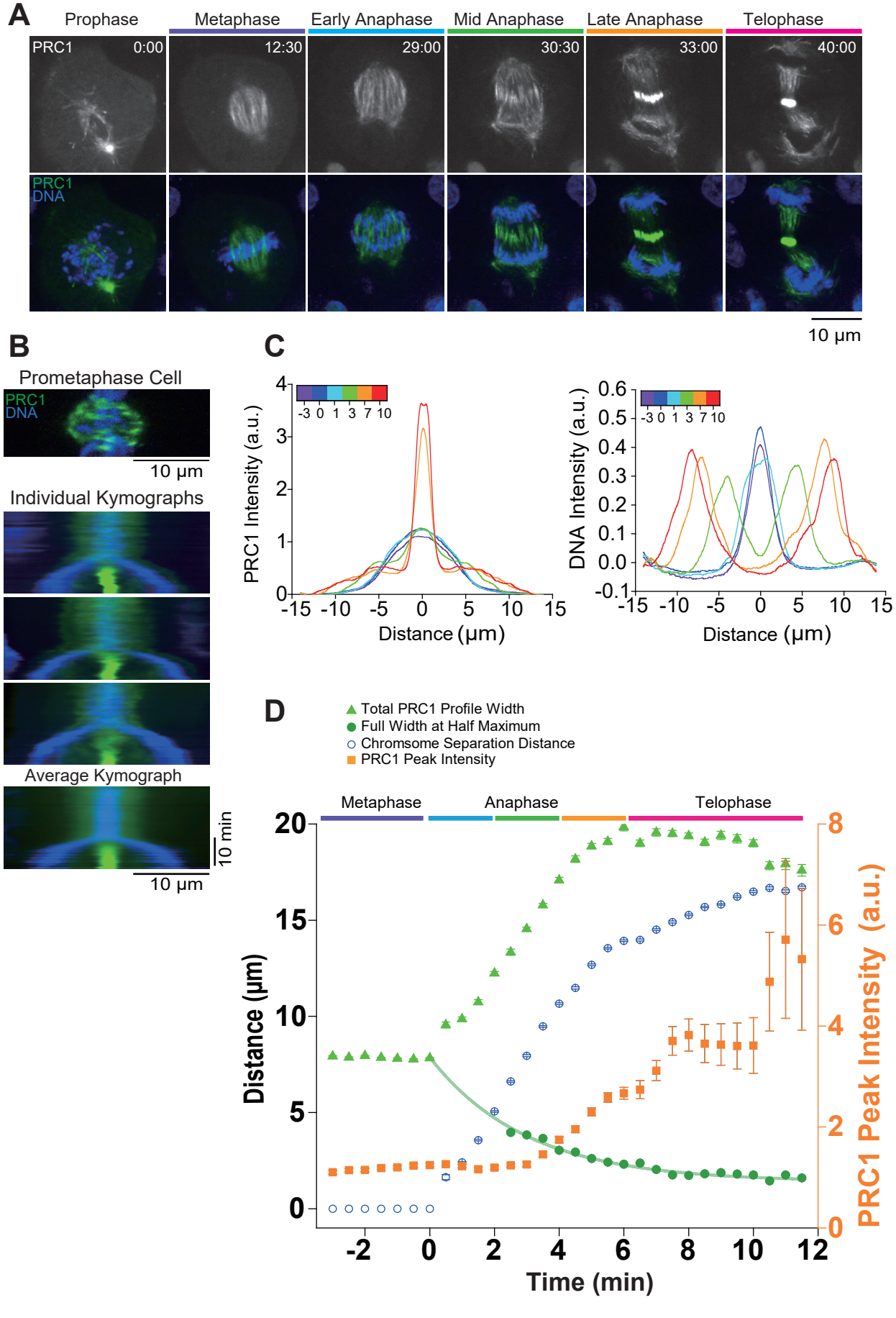

Figure 2

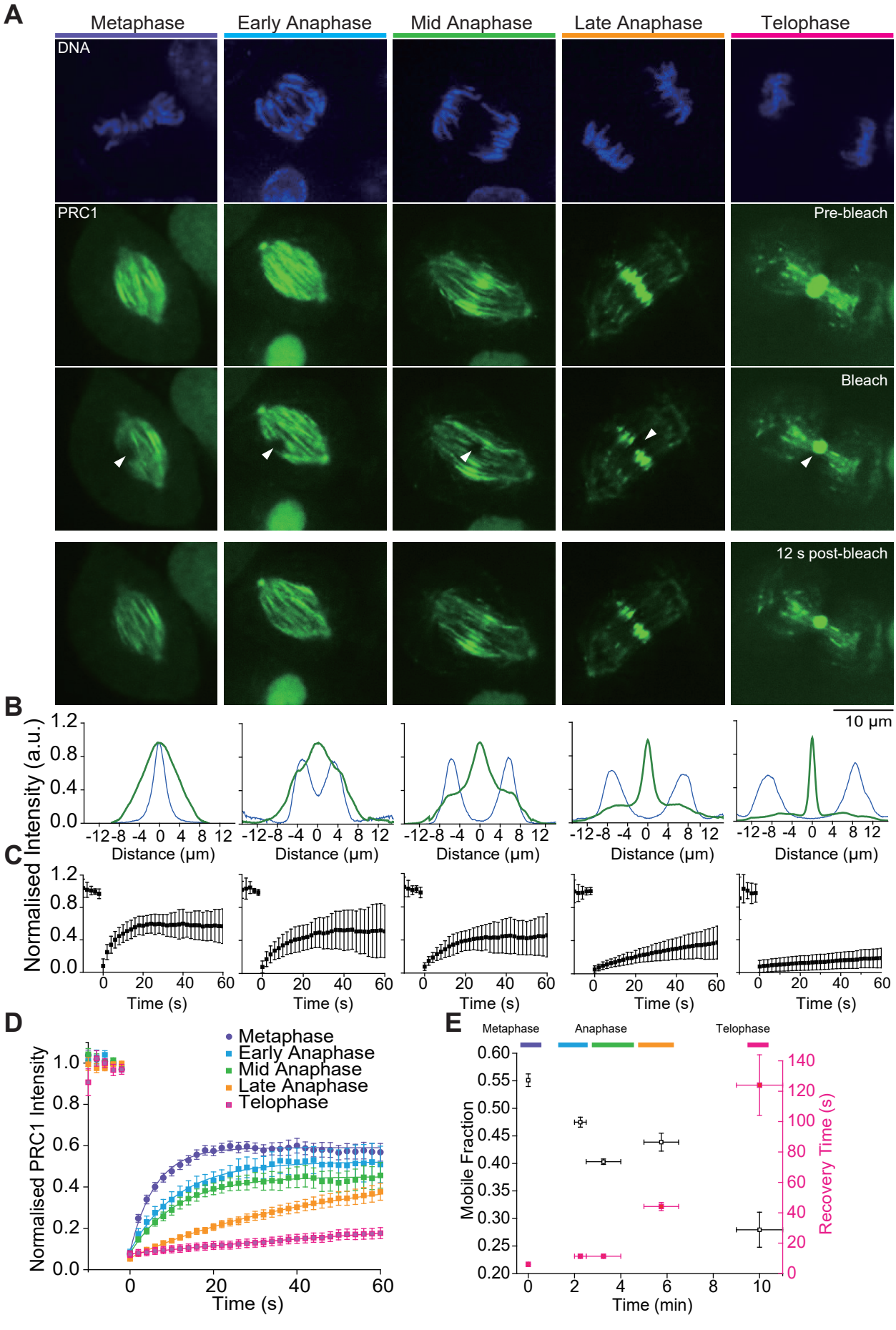

Figure 3

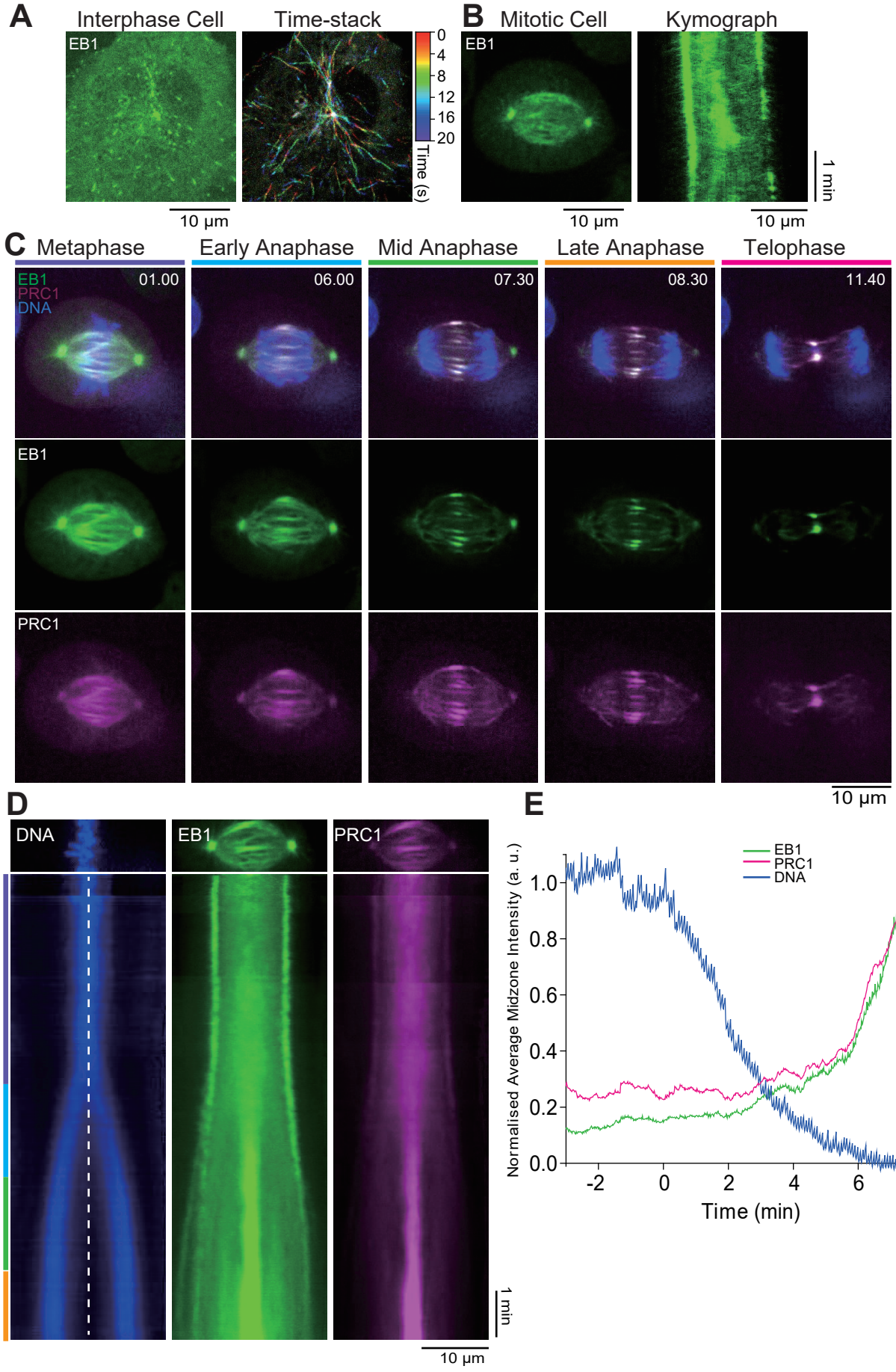

Figure 4

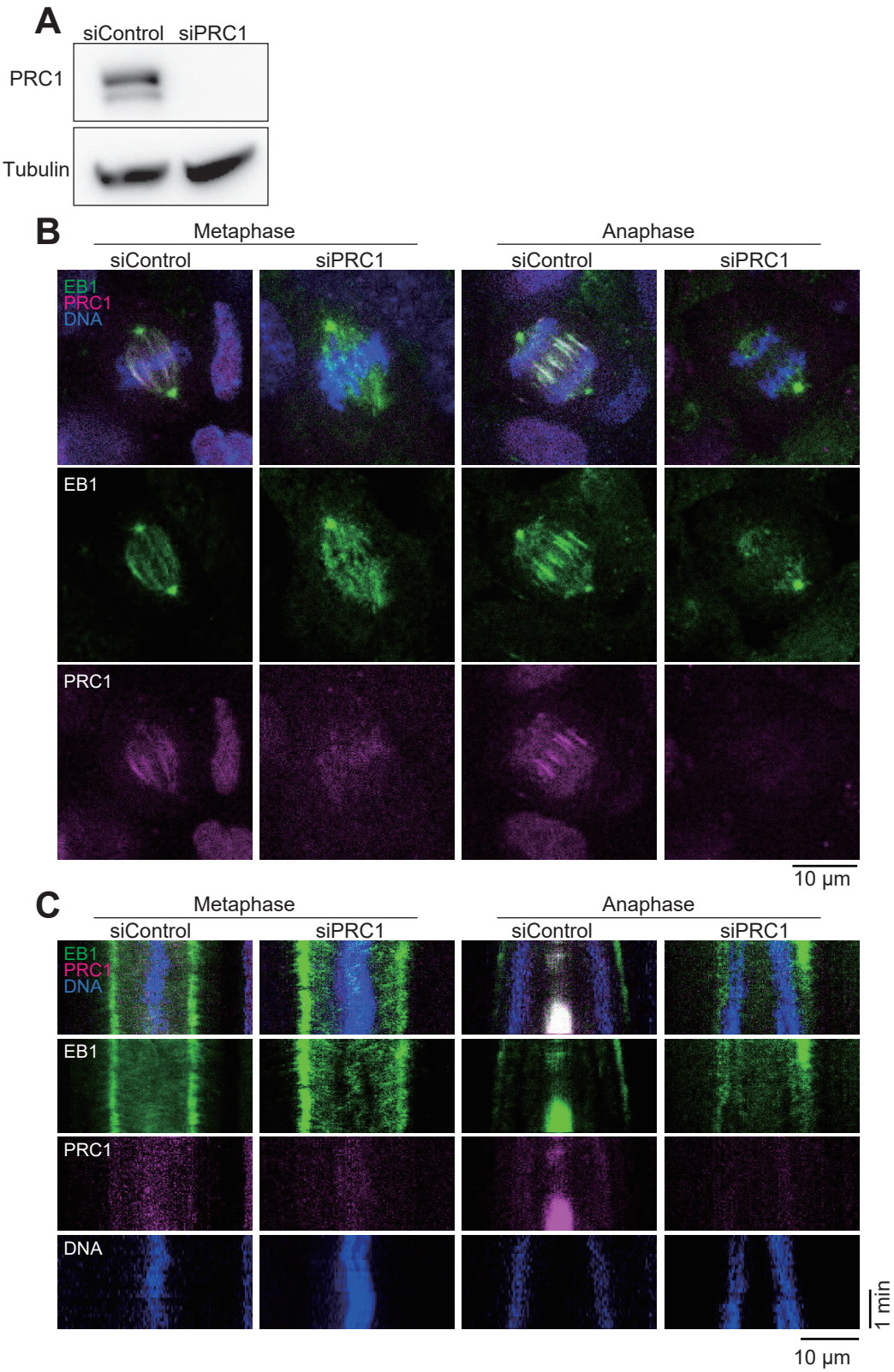

Figure 5

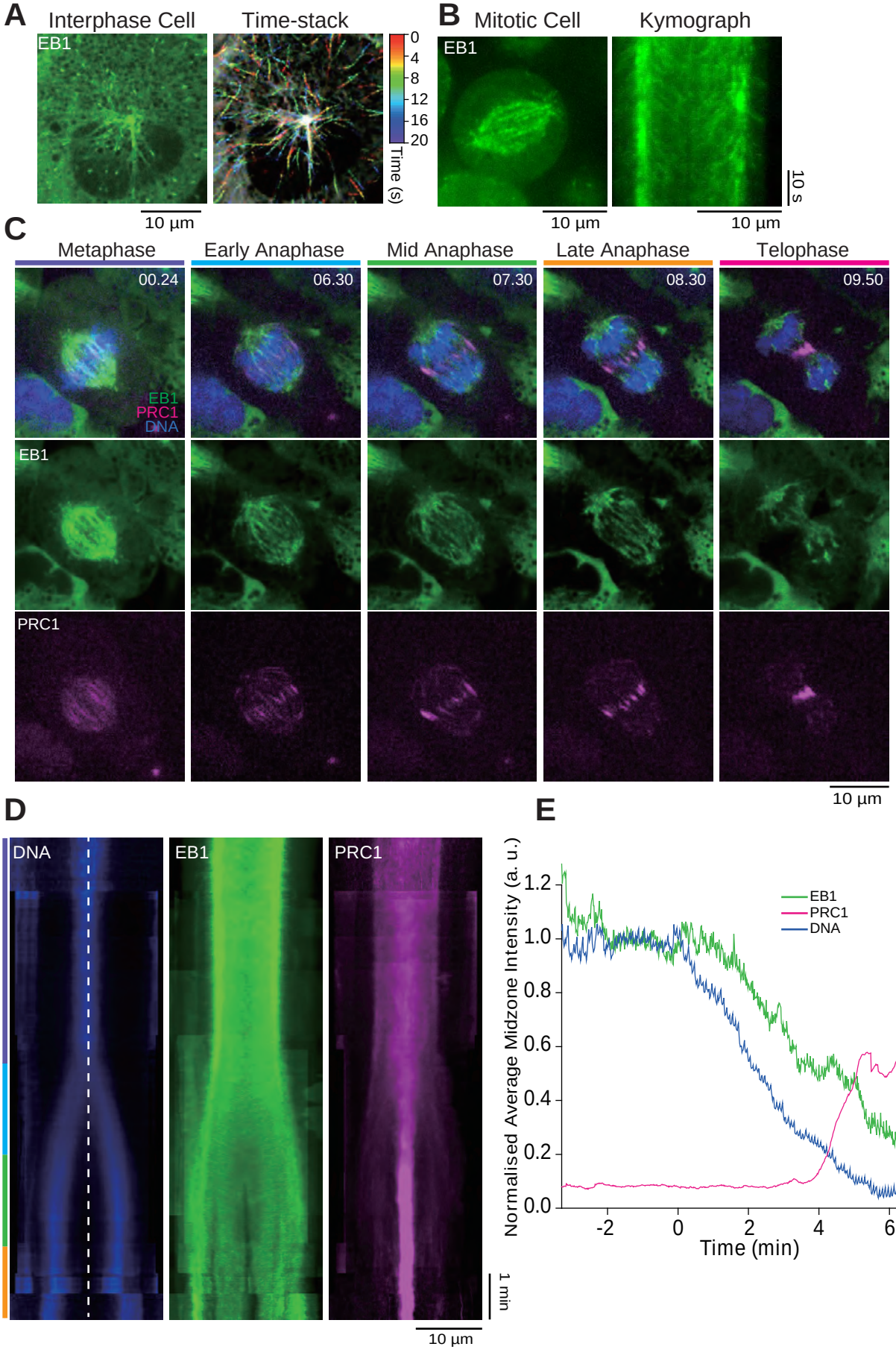

Figure 6